Distribution of magnetic flux on the solar surface and low-degree p-modes

F. Moreno-Insertis[1,2]★ and S. K. Solanki[3]★

[1]*Instituto de Astrofísica de Canarias, 38200 La Laguna, Tenerife, Spain*
[2]*Department of Astrophysics, Facultad de Fisica, Universidad de La Laguna, 38200 La Laguna, Tenerife, Spain*
[3]*Institute of Astronomy, ETH-Zentrum, CH-8092 Zurich, Switzerland*

ABSTRACT

The frequencies of solar p-modes are known to change over the solar cycle. There is also recent evidence that the relation between frequency shift of low-degree modes and magnetic flux or other activity indicators differs between the rising and falling phases of the solar cycle, leading to a hysteresis in such diagrams. We consider the influence of the changing large-scale surface distribution of the magnetic flux on low-degree ($l \leq 3$) p-mode frequencies. To that end, we use time-dependent models of the magnetic flux distribution and study the ensuing frequency shifts of modes with different order and degree as a function of time. The resulting curves are periodic functions (in simple cases just sine curves) shifted in time by different amounts for the different modes. We show how this may easily lead to hysteresis cycles comparable to those observed. Our models suggest that high-latitude fields are necessary to produce a significant difference in hysteresis between odd- and even-degree modes. Only magnetic field distributions within a small parameter range are consistent with the observations by Jiménez-Reyes et al. Observations of p-mode frequency shifts are therefore capable of providing an additional diagnostic of the magnetic field near the solar poles. The magnetic distribution that is consistent with the p-mode observations also appears reasonable compared with direct measurements of the magnetic field.

Key words: Sun: activity – Sun: magnetic fields – Sun: oscillations.

1 INTRODUCTION

Observations have convincingly shown that solar p-mode frequencies are increased by magnetic activity (Woodard & Noyes 1985; Libbrecht & Woodard 1990; Elsworth et al. 1990, 1994; Bachmann & Brown 1993; Rhodes et al. 1993; Pallé 1994; Jiménez-Reyes et al. 1998). Both low- ($l = 0$–3) and intermediate-degree ($l \approx 5$–150) modes are affected, and the relative change in frequency between solar activity minimum and maximum is of order $0.4\,\mu$Hz.

A number of proposals have been advanced to explain the observed frequency shifts. Libbrecht & Woodard (1990) and Woodard et al. (1991) have argued on the basis of observations of intermediate-degree modes that the source of the perturbations must lie near the solar surface. This conclusion is supported by Gough & Thompson (1988a,b), Vorontsov (1988) and Paternò (1990), who have found that magnetic fields with strengths significantly below 10^6 G located near the bottom of the convection zone have an unobservably small influence on p-modes. However, fields with strengths significantly larger than 10^5 G cannot be stably stored in these layers (Moreno-Insertis, Schüssler & Ferriz-Mas 1992; Schüssler et al. 1994). Consequently, we consider here only magnetic fields at or very near the solar surface.

Kuhn (1988) invoked sound-speed changes caused by excess heating in the solar atmosphere and interior to explain frequency splittings between modes of different azimuthal order m. Goldreich et al. (1991) point out, however, that the main influence of a temperature variation is to change the path-length, while the propagation speed is affected most strongly by the magnetic field. By requiring that the thermal changes contributing to the frequency shifts, $\delta\omega$, of intermediate-degree modes should be consistent with measured irradiance variations (e.g. Willson & Hudson 1991; Kyle, Hoyt & Hickey 1994; Fröhlich & Lean 1998), they determine that the major influence must be that of the field, specifically of vertical magnetic flux tubes. The associated temperature change does, however, improve the correspondence with the data. The influence of thin magnetic fibrils (flux tubes) has been investigated in greater detail by, e.g., Bogdan & Zweibel (1985) for an unstratified atmosphere and by Zweibel & Däppen (1989) in a stratified atmosphere, without, however, attempting to reproduce specific observations.

Evans & Roberts (1990, 1991, 1992) proposed that the horizontal magnetic field in the chromospheric canopy created by the expansion of small flux tubes is the source of intermediate-degree mode frequency shifts (cf. Wright & Thompson 1992). Jain & Roberts (1993) have extended this analysis to include temperature changes in the chromospheric canopy, which improve the

★ E-mail: fmi@ll.iac.es (FMI); solanki@astro.phys.ethz.ch (SKS)

fit to the $\delta\omega$ of the high-frequency modes. Finally, a more speculative approach has been taken by Lydon, Guenther & Sofia (1996), who postulate a horizontal field of some 100-G strength located roughly 300 km below the solar surface. They contend that it changes in strength by 400 G over the solar cycle and leads to the observed frequency changes. However, they give no convincing arguments as to how such a field can be stored there without erupting to the surface.

The above investigations have all explicitly or implicitly assumed the solar magnetic field to be homogeneously distributed over the solar surface (at least on large scales). Full-disc magnetograms and synoptic maps reveal, however, that this is patently not the case. In the framework of a perturbation approach, Gough & Taylor (1984) and Gough & Thompson (1990) have worked out in detail how a magnetic field affects p-modes. These authors also included the latitude distribution of the magnetic flux in their treatment. This distribution of the perturber (assumed to affect only the sound speed) was reconstructed from frequency splittings of intermediate-degree modes by Gough (1988), Kuhn (1988), Libbrecht & Woodard (1990) and Woodard & Libbrecht (1993). Shibahashi (1997) showed that the magnitude of the observed frequency change of low-degree modes over the solar cycle is compatible with the extrapolation from the observed intermediate-degree mode frequency shift if the sound-speed perturbations are restricted to low latitudes. Dziembowsky & Goode (1997) also considered this problem, but were mainly interested in recovering the signal of the deep interior and removing the disturbance due to a surface magnetic field.

In the present paper we go a step further in the modelling of low-degree frequency shifts. We investigate the influence on the p-mode frequencies of the evolution over the solar cycle of the distribution over latitude of magnetic flux. We are interested in the relationship between oscillation frequency and activity indicators such as longitudinal magnetic flux or sunspot number, as have been observationally analysed by Elsworth et al. (1990), Woodard et al. (1991), Bachmann & Brown (1993), Rhodes et al. (1993) and Jiménez-Reyes et al. (1998). Of particular relevance are the recently published variations and correlations with total longitudinal magnetic flux of low-degree p-mode frequencies observed over the whole of solar cycle 22 (Jiménez-Reyes et al. 1998). The frequencies are seen to increase during the rising phase of the solar cycle, and to decrease again during the declining phase. When plotted against the magnetic flux, however, they do not follow the same path in the rising and declining phases, i.e., they show a hysteresis. There is also some evidence that this hysteresis is different for odd- and even-degree modes.

In this paper we show how the hysteresis may easily result from the phase shift between the time evolution curves of the frequency of p-modes with different degree and order l, m. Given their spatial distribution, the sectoral and zonal modes have a different sensitivity for the presence of magnetic flux in the different latitudes. The surface magnetic flux distribution, on the other hand, does not reach its maximum at the same time in the different latitudes. The combination of these two effects causes the frequency of the p-modes to describe a roughly sinusoidal curve in time, so that two such curves for p-modes with different l and m are shifted in time by an amount which depends on the respective sensitivity of those modes to the equatorial and polar fields. A plot of the two frequency curves versus each other along time must thus show a hysteresis. If a given activity indicator basically depends on (or is correlated with) the magnetic flux distribution at a limited range of latitudes only, then a hysteresis can also appear when plotting

the frequency shift of one mode against that activity indicator. In this paper we show that this effect is amenable to a detailed analytical description, and how the results thereby obtained bear a strong resemblance to the observational findings.

In the following we concentrate on low-degree modes, in spite of the disadvantage they suffer of not being able to provide the same amount of surface detail as higher degree modes. There are (at least) three reasons for this. First, there is a large body of high-quality data available for those modes. It stretches from 1984 to the present and forms the longest *uninterrupted* helioseismological time series obtained from any one site (except for the diurnal and occasional weather- or instrument-related interruptions). Secondly, the low-degree modes are the only ones detectable without resolving the solar disc. Hence these modes are the only ones which may in future provide us with any information on stellar magnetism and its surface distribution. Thirdly, it is important to remove accurately all influences of surface magnetism from these mode frequencies before using them to infer the structure of the deep solar interior, as was demonstrated by Dziembowski et al. (1997).

2 FREQUENCY SHIFT FOR INDIVIDUAL VALUES OF l AND m

To use the hysteresis observations as a diagnostic tool we have to obtain an expression for the frequency shift of the low-l p-modes (say, $l \leq 3$) that follows from a given distribution of magnetic flux on the solar surface. As a first approximation, we mimic the effect of the magnetic elements on the modes by assuming a perturbed distribution of the sound speed of the form

$$c(r, \theta) = c_0(r) + \delta c(r, \theta), \tag{1}$$

and take the perturbation δc to be a simple function of the field distribution. In equation (1), r is the radial coordinate, θ is the co-latitude, and $c_0(r)$ is the unperturbed, spherically symmetric sound-speed distribution. Following the observational evidence (Libbrecht & Woodard 1990; Woodard et al. 1991), $\delta c(r, \theta)$ will be taken as different from zero only in the surface layers. In addition, we neglect the possible dependence of δc on the azimuthal angle ϕ, and consider instead axisymmetric perturbations. This is allowed since we do not expect any preferred longitudes to persist over significant fractions of the solar cycle and the observational results should also correspond to ϕ-independent time averages. These simplifications have the advantage that one can then obtain the corresponding frequency shifts by using a relatively simple theory of degenerate perturbations (e.g. Gough & Thompson 1990). Additionally, for the modes used in the observational study (with $l \leq 3$ and n typically between 12 and 30), one can use the JWKB asymptotic theory (Vandakurov 1967; Tassoul 1980). The frequency shift, $\delta\omega_{nlm}$, caused by the perturbation δc in a mode with unperturbed frequency ω_{nl} can then be written as

$$\frac{\delta\omega_{nlm}}{\omega_{nl}} = \frac{1}{S_{nl}} \int_0^R K_{nl}(r) H_{lm}(r) \, dr, \tag{2}$$

with

$$H_{lm}(r) = \left(l + \frac{1}{2}\right) \frac{(l-m)!}{(l+m)!} \int_0^\pi |P_l^m(\cos\theta)|^2 \frac{\delta c(r, \theta)}{c_0(r)} \sin\theta \, d\theta, \tag{3}$$

$$K_{nl}(r) = \frac{1}{c_0} \left(1 - \frac{c_0^2}{r^2} \frac{L^2}{\omega_{nl}^2}\right)^{-1/2}, \tag{4}$$

and

$$S_{nl} = \int_{r_t}^{R} \frac{1}{c_0} \left(1 - \frac{c_0^2}{r^2} \frac{L^2}{\omega_{nl}^2} \right)^{-1/2} dr. \tag{5}$$

In the foregoing equations, P_l^m are Legendre polynomials, $L^2 = (l+1)l$, R represents the solar surface, and r_t is the lower turning point for the unperturbed mode considered.

To progress, we have to separate the radial and angular dependence of c. If, by assumption, the perturbations in c are related to solar surface magnetism (i.e., the distribution of magnetic canopy field strengths and base heights or of magnetic elements on the solar surface), we expect no strong correlation between the r and the θ dependences of c.[1] We can thus write, as a first approximation,

$$\delta \log c(r, \theta) = f(r) h(\theta), \tag{6}$$

where $f(r) \geq 0$ and is different from zero only close to the surface, and h is related to the (time-dependent) surface distribution of the magnetic field. For the range of n and l seen in observations not resolving the solar disc, the radial integral in equation (2) simplifies to a value independent of n (see, e.g., Gelly et al. 1997 for observational support for this approach). To match the observational results, we have to average the other quantities appearing in equation (2) over the range of values of n considered. We call $\delta \omega_{lm}$ the n-averaged frequency shift, and obtain

$$\delta \omega_{lm} = A \bar{f} I_{lm}, \tag{7}$$

with A the n-average of ω_{nl}/S_{nl},

$$I_{lm}(t) = \left(l + \frac{1}{2} \right) \frac{(l-m)!}{(l+m)!} \int_0^{\pi} |P_l^m(\cos\theta)|^2 h(\theta, t) \sin\theta \, d\theta, \tag{8}$$

and $\bar{f}$ the radial average of $f(r)$ with the weighting function $c_0^{-2}(r)$. All variables in equation (7) except A and (to first order) $\bar{f}$ are time-dependent on the time-scale of the evolution of the surface distribution of the solar magnetic field. A can also be taken to be l-independent, since the mode inertia for the low-l modes considered here does not vary substantially with l (for a definition of the mode inertia, see, e.g., Christensen-Dalsgaard 1998). Equation (7) thus states that the differences in frequency perturbation for the different (l, m) values are basically contained in the angular integral I_{lm} of (8). In the following paragraphs we study the time behaviour of I_{lm} for different (l, m) pairs, thereby obtaining time profiles of $\delta \omega_{lm}$. We show that, when plotted against an activity indicator, they yield hysteresis cycles of different widths and signs depending on the value of l and m and the latitude and time dependence of $h(\theta, t)$, which is a function of the magnetic field on the solar surface. $h(\theta, t)$ must be strictly positive to ensure that mode frequencies increase with magnetic flux, as dictated by the observations. Since we do not explicitly calculate A, we do not predict absolute values for $\delta \omega_{lm}$. For this reason we always normalize $\delta \omega_{lm}$ to the maximum value reached by the most strongly affected mode.

To calculate the integrals in (8), we first need to model the surface distribution of magnetic field along the cycle (Section 3).

[1] There may be a different r dependence of δc within sunspots and magnetic elements due to their different temperatures and sizes. Since sunspots are restricted to zones within 30° of the equator, a certain correlation between the r and θ dependence of δc may hence be introduced. This, however, is a second-order effect and goes beyond the scope of the present paper.

From it, we then have to obtain the input function $h(\theta, t)$ (Section 4.1). We consider only (l, m) values which yield symmetric modes about the equator (i.e., those with even $l - m$), since only these are detected in disc-integrated observations.

3 SURFACE DISTRIBUTION OF MAGNETIC FLUX AND ACTIVITY INDICATORS

We need a description of the longitudinally averaged distribution of the unsigned solar surface magnetic flux which must fulfil the following three criteria: it must be simple, possess some realism, and be easily adaptable to numerical experiments. We start with the expansion of the azimuthally averaged magnetic flux, let us call it $b(\theta, t)$, in terms of Legendre polynomials due to Stenflo (1994):

$$b(\theta, t) = \sum_{l'} a_{l'} P_{l'}(\cos\theta) \cos[\omega_{cyc}(t - t_{l'})], \tag{9}$$

with ω_{cyc} the frequency of the solar magnetic cycle, i.e., $\omega_{cyc} = 2\pi/T_{cyc}$, $T_{cyc} = 22$ yr, and $\omega_{cyc} t_{l'}$ an l'-dependent phase. Only the odd-l' modes with $1 \leq l' \leq 13$ are included in this expansion. Note that the azimuthal averaging leaves only the net flux per latitude band. This distribution clearly shows the evolution of the activity belts at low latitudes over the solar cycles. It also exhibits considerable net flux at high latitudes, which starts near the activity belts and drifts towards higher latitudes in the course of the cycle, forming strong polar caps at activity minimum. The main advantage of the azimuthally averaged fields described by Stenflo (1994) is their near-independence of the spatial resolution of the observations. Their main disadvantage is that the p-mode frequencies depend on some power of the unsigned magnetic field $B(\theta, t)$ derived from full-disc magnetograms, which is a related but distinct quantity.

We expect $B(\theta, t)$ to differ quantitatively from $b(\theta, t)$, but to display the same qualitative θ and t dependence. The main quantitative difference is that whereas azimuthally averaged net flux at high latitudes is almost as large as in the activity belts, the amount of unsigned magnetic flux decreases significantly with latitude (Howard & LaBonte 1981), although considerably enhanced magnetic flux is observed at the poles around solar activity minimum (Stenflo 1970; Svalgaard, Duval & Scherrer 1978; Giovanelli 1982; Sheeley, Wang & Harvey 1989; Zhang, Zirin & Marquette 1997). The observations of $B(\theta)$ derived from full-disc magnetograms suffer heavily from their insensitivity to the transverse components of the magnetic field, their limited spatial resolution (leading to underestimates of the mixed polarity fields dominating, e.g., the quiet network) and the low signal levels near the limb, so that the signals of smaller magnetic features drown in the noise there. These effects lead to considerable uncertainty in the true $B(\theta)$. Estimates of high-latitude and polar fields suffer most gravely.

In view of the above uncertainties, we expect the true $B(\theta)$ distribution to lie somewhere between that of Stenflo (1994) and that suggested by the analysis of Stenflo (1972) and Howard & LaBonte (1981). We take this into account by modifying Stenflo's distribution in a simple, parametrized manner:

$$B(\theta, t) = |[\cos^n q(\pi/2 - \theta)] b(\theta, t)|, \tag{10}$$

where n and q are free parameters. They may be varied in order to test the influence of different magnetic field distributions and evolutions on the p-mode frequencies. In general, we have chosen
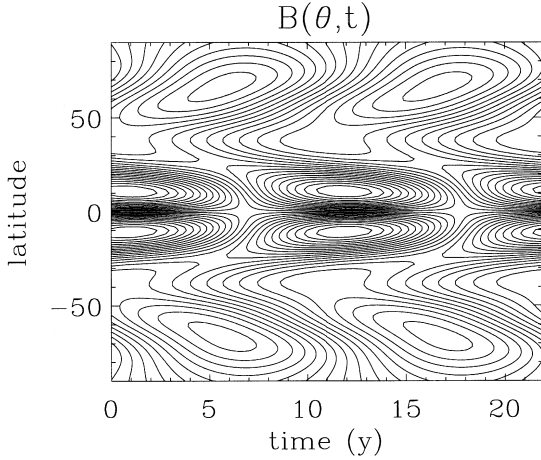
Figure 1. Evolution of the latitude dependence of the unsigned magnetic flux $B(\theta, t)$ over a solar magnetic cycle for $n = 2$ and $q = 0.7$.

values of $n = 0, 1, 2$ and $0 \leq q \leq 2$. A contour plot of a sample $B(\theta, t)$ distribution over a solar cycle is plotted in Fig. 1 for the parameters $n = 2$ and $q = 0.7$, which, as explained in later sections, is a particularly convenient choice.

Additionally, in order to estimate the influence of the active latitudes (between $\pm 30°$) on p-mode frequencies, we have also considered a case in which

$$B(\theta, t) = \begin{cases} |b(\theta, t)| & \text{for } 60° \leq \theta \leq 120°, \\ 0 & \text{otherwise.} \end{cases} \tag{11}$$

We stress that $B(\theta, t)$ is not the true field strength, but only a measure of the field strength after spatially averaging over each θ bin. Its relation to the true intrinsic B depends on the type of magnetic feature considered. For small-scale magnetic elements the intrinsic field strength is usually the same (i.e., it lies within a small range; cf. Rüedi et al. 1992; Solanki et al. 1996), so that $B(\theta, t)$ is proportional to the magnetic filling factor or flux. For magnetic canopies in the low solar chromosphere $B(\theta, t)$ is proportional to the actual field strength in the canopy.

The behaviour of $\delta\omega_{lm}$ versus some proxy of solar activity is of particular interest. For illustration we consider two proxies, namely the sunspot number R_Z and the total longitudinal magnetic flux. They are related to $B(\theta, t)$ in the following manner.

Consider first the Zürich sunspot relative number, R_Z. Sunspots are confined to the activity belts, and $R_Z(t)$ increases with increasing magnetic flux in these belts (equation 11). There is no simple proportionality between the two, however, since the ratio of magnetic flux in sunspots to that in the whole active region increases with increasing active region flux, although the exact details of this dependence are not certain. Helpful are the related observations of Chapman, Cookson & Dobias (1997) of the ratio of the total area of sunspots and of (active region) faculae during the declining phase of cycle 22. They show that this ratio decreases roughly linearly from activity maximum to minimum. Taking this into account, we approximate R_Z as:

$$R_Z(t) = R_0 \int_{60°}^{120°} B^2(\theta, t) \, \mathrm{d}\theta, \tag{12}$$

where R_0 is a conversion constant, chosen here to be 150. The results do not depend on the choice of R_0. According to Bachmann & White (1994) and others, the sunspot number and the 10.7-cm

flux used by Jiménez-Reyes et al. (1998) are very closely related in their temporal behaviour. In particular, the time lag between the two quantities is only $20 \pm 5\,\mathrm{d}$.

The total amount of longitudinal flux in a synoptic chart produced from magnetograph measurements (which is the quantity used by Jiménez-Reyes et al. 1998 to compare with the frequency shifts) can be related to the unsigned field in a synoptic map like Fig. 1 as follows:

$$|B_{\|,\mathrm{tot}}| \sim \int |B(\theta, t)| D(\theta) \sin\theta \, \mathrm{d}\theta, \tag{13}$$

where $\sin\theta$ takes into account the sensitivity of magnetographs to the longitudinal component of the field only, and $D(\theta)$ is a function which takes into account the visibility of mixed polarity magnetic fields at finite spatial resolution. (The foreshortening near the limb need not be taken into account when constructing a synoptic map, since this effect is exactly compensated by the over-representation of high latitudes.) $D(\theta)$ must obviously decrease towards the poles, since due to foreshortening the effective surface area sampled on the Sun for a fixed angular pixel size increases as $1/\sin\theta$ (if the curvature of the solar surface at the very limb is neglected). The exact shape of $D(\theta)$ depends on the size distribution of patches of monopolar magnetic field relative to the pixel size at disc centre. We shall choose here for illustrative purposes

$$D(\theta) = 1 + \sin\theta. \tag{14}$$

This is roughly the form one obtains if the distribution of sizes of monopolar magnetic patches follows a power law with exponent -2.

4   FREQUENCY SHIFTS

4.1   Sound-speed perturbation

In line with the arguments of previous authors (e.g. Gough & Thompson 1988a,b; Libbrecht & Woodard 1990), we assume that the magnetic field distribution $B(\theta, t)$ of the foregoing section causes a sound-speed perturbation of the form described by equation (6). Given the uncertainty in the type of magnetic features responsible for the frequency perturbations (i.e., magnetic flux tubes or canopies), it is unclear whether δc should be proportional to approximately B^2 (in the case of canopies) or directly to B (for kG flux tubes). This is particularly true on the long time-scales we are interested in here (on somewhat shorter time-scales, Woodard et al. 1991 have found evidence in favour of a proportionality with B). We thus take

$$h(\theta, t) = K B^{i_b}(\theta, t), \tag{15}$$

and allow i_b to adopt a few different values (e.g., 1 or 2) in the calculations presented in the following. In equation (15), K is a normalization constant.

4.2   Time variation of the frequency shifts

The latitude of the maximum of the field distribution $B(\theta, t)$ changes with time. If this latitude happens to coincide with the latitude of the maximum of a p-mode, the influence of B on this particular mode will be largest. Conversely, when the latitude of the maximum of B coincides with a node, the influence will be minimized. Hence, two p-modes with nodes and maxima at different latitudes will yield time distributions of the cyclic

integral $I_{lm}(t)$ (equation 8) which are phase-shifted in time relative to each other. This phase delay will thus be apparent in the corresponding frequency shifts $\delta\omega_{lm}$. For example, the polar field reaches its maximum and minimum several years after the field in active latitudes. Depending on the relative sensitivity of each given P_l^m for the polar or equatorial regions, the resulting I_{lm} will be shifted in time by an amount which depends on (l, m).

The sampling capability of the different (l, m) modes can be studied analytically when we adopt $i_b = 2$ in equation (15) and use any magnetic distribution $B(\theta, t)$ with a sinusoidal profile in time at each latitude, like the distributions of equations (9) and (10). In that case, each integral $I_{lm}(t)$ also has a sinusoidal profile in time. This can be seen as follows: assume $B(\theta, t)$ to have the following general shape:

$$B(\theta, t) = \mathcal{A}(\theta)\cos\{\omega_{\mathrm{cyc}}[t - \tau(\theta)]\}, \qquad (16)$$

the *time lag* $\tau(\theta)$ being a smooth function of the latitude. Values for $\mathcal{A}(\theta)$ and $\tau(\theta)$ for the field distribution of Fig. 1 are given in Fig. 2. In the particular case of the distributions (10) or (11) based on expression (9), it is straightforward to convert $B(\theta, t)$ into an expression of the form (16). In that case, both $\mathcal{A}$ and τ have contributions from all l'-modes in $b(\theta, t)$. Using now (15) to calculate $h(\theta, t)$, the $I_{lm}(t)$ integrals (and, therefore, the frequency shifts $\delta\omega_{lm}$; see equation 7) can be easily expressed in the form of an exact sinusoidal function of period $T_{\mathrm{cyc}}/2$ and phase shift
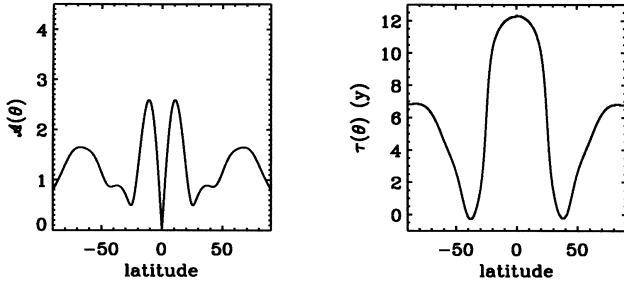
Figure 2. Amplitude and phase of the field distribution of Fig. 1 as given in equation (16).
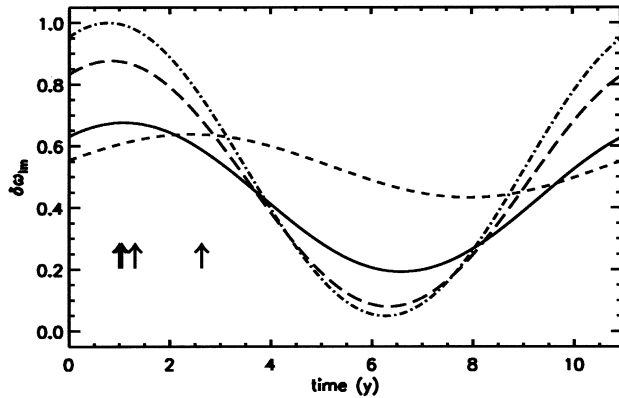
Figure 3. The $\delta\omega_{lm}(t)$, or, equivalently, the integrals $I_{lm}(t)$ for modes with $l \leq 2$ over a complete solar cycle. The $\delta\omega_{lm}$ are normalized to the maximum value reached by the plotted modes. The line styles are: $(l, m) = (0, 0)$ solid; $(1, 1)$ long-dashed; $(2, 0)$ short-dashed; $(2, 2)$ dot-dashed. In the lower part of the figure we have indicated the epoch of the respective $\delta\omega_{lm}$ maxima as vertical arrows. The underlying $B(\theta, t)$ has $n = 2$ and $q = 0.7$ (equation 10). A quadratic dependence of δc on B has been assumed, i.e., $i_b = 2$ in equation (15).

$2\omega_{\mathrm{cyc}}T_{lm}$:

$$I_{lm}(t) = U_{lm} + |\mathcal{J}_{lm}|\cos[2\omega_{\mathrm{cyc}}(t - T_{lm})], \qquad (17)$$

with $\mathcal{J}_{lm}$ a complex amplitude defined as

$$\mathcal{J}_{lm} = \frac{K}{2}\left(l + \frac{1}{2}\right)\frac{(l - m)!}{(l + m)!}$$
$$\times \int_0^\pi |P_l^m(\cos\theta)|^2 \mathcal{A}^2(\theta)\exp[2i\omega_{\mathrm{cyc}}\tau(\theta)]\sin\theta\,\mathrm{d}\theta, \qquad (18)$$

K being the normalization constant of equation (15), and T_{lm}, the *time lag of the (l, m) mode*, given by the complex phase of $\mathcal{J}_{lm}$, viz.

$$T_{lm} = \frac{1}{2\omega_{\mathrm{cyc}}}\arccos\left[\frac{\mathrm{Re}(\mathcal{J}_{lm})}{|\mathcal{J}_{lm}|}\right]. \qquad (19)$$

In equation (17), U_{lm} is just a global time-independent shift of the curve $I_{lm}(t)$, given again by (18) but without the exponential factor in the integrand. Equations (18) and (19) directly show how the time lag of each p-mode results from an average of the individual time lags at each latitude with weighting function $|P_l^m(\cos\theta)|^2\mathcal{A}^2(\theta)$.

An example of the $\delta\omega_{lm}(t)$ obtained in this manner for $l \leq 2$ over a solar cycle is plotted in Fig. 3 for $n = 2$ and $q = 0.7$. As can be seen, the amplitudes of $\delta\omega_{lm}$ depend on l and m. The $\delta\omega_{lm}$ also exhibit relative phase shifts, with the maxima of the zonal modes $(0, 0)$ and $(2, 0)$ lying 5 months and 1.7 years, respectively, after the maxima of the sectoral modes. In this figure all modes, but in particular the zonal modes, show significant shifts $\delta\omega_{lm}$ even around activity minimum. This is due to the fields at high latitudes and in particular the poles, which are most prominent near activity minimum.

Now, activity indicators such as the longitudinal magnetic flux or sunspot number are also cyclical functions whose maxima need not coincide with those of $\delta\omega_{lm}$. Indeed, for the examples displayed in Fig. 3 it is not possible for any single activity indicator to have maxima coincident with all the modes concurrently. If we now plot the normalized frequency shifts versus some activity indicator, we then expect to obtain hysteresis cycles (more precisely, Lissajous figures) for those modes whose time of maximum $\delta\omega_{lm}$ does not coincide with those of the activity indicators. If the maximum in time of the chosen activity indicator is located at least some months before or after those of the $\delta\omega_{lm}$ curves, then the obtained cycles will exhibit a noticeable hysteresis. This is described in the following subsection.

5 HYSTERESIS CYCLES

5.1 Analytical estimates and numerical results

Let us first use as activity indicator our simple estimate of R_Z given in Section 3 (equation 12). If we plot the same frequency shifts $\delta\omega_{lm}$ for the individual values of l and m already shown in Fig. 3 but now versus R_Z, we obtain the diagram shown in the upper panel of Fig. 4. For easiness of reference later on in the paper, we have multiplied the frequency shift of each mode by the visibility function v_{lm} given by, e.g., Christensen-Dalsgaard (1989). Line styles of the individual modes are the same as in Fig. 3; the thicker sections of the curves correspond to the rising half of the cycle (i.e., R_Z increasing with time). The plotted curves clearly exhibit a hysteresis: $\delta\omega_{lm}$ does not follow the same path in the rising and falling parts of the solar cycle.

The hysteresis cycles shown in Fig. 4 will be said to have *positive* circulation sense when the frequency shift $\delta\omega_{lm}$ is smaller in the rising half of the cycle than in the declining half (clockwise
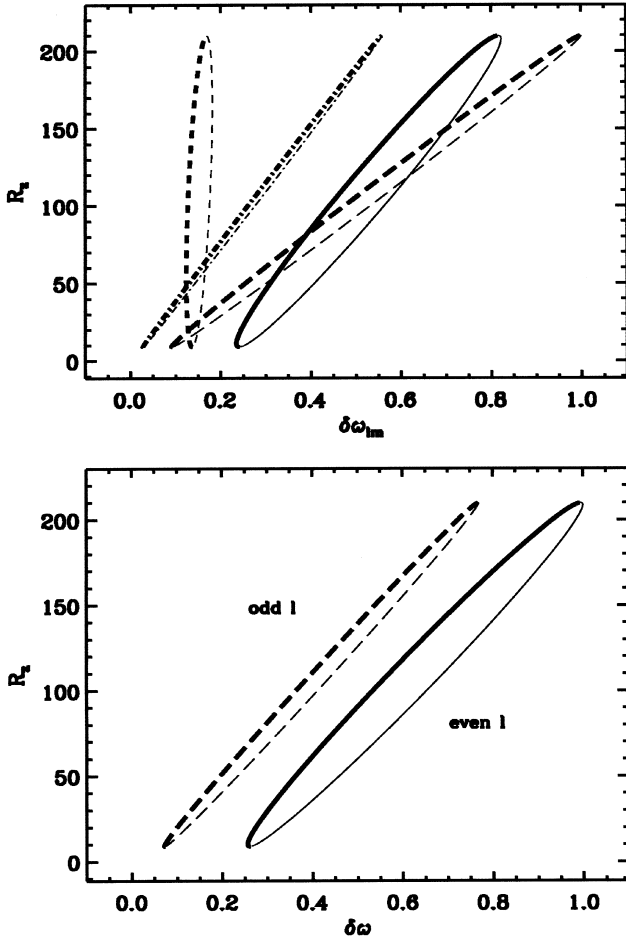
Figure 4. Hysteresis cycles obtained using the relative sunspot number defined following equation (12) as activity indicator and parameters $i_b = 2$, $n = 2$ and $q = 0.7$. Upper panel: cycles for the individual modes; line styles as for Fig. 3. Lower panel: cycles obtained for all odd-l (long-dashed) and even-l (solid) together; the thicker stretches of the curves correspond to the rising part of the solar activity cycle. All frequency shifts have been multiplied by the visibility function v_{lm}, as explained in the text.

circulation of the cycle). Similarly, we will say that the inclination of a cycle is *positive* (or that it is *forward inclined*) if the long axis of the ellipse lies in the first and third quadrants of the coordinate frame; otherwise the inclination will be called *negative* (and the cycle will be said to be *backward inclined*). All modes shown in the figure have positive circulation sense and are forward inclined. This can also be predicted analytically through an elementary analysis. As in equation (17), assume the time evolution of $\delta\omega_{lm}$ to be a sinusoidal curve with amplitude $|\mathcal{J}_{lm}|$, and with the maximum occurring at time T_{lm}. Similarly, let us call A_R and t_R the amplitude and time of maximum of the activity indicator. If the latter were a sinusoidal curve (which is exactly true for the activity indicator used in the figure, but only approximately correct for other indicators), then we obtain an elliptical cycle with circulation sense s_{lm}, inclination sign α_{lm} and *normalized width* w_{lm} given by

$$
\begin{cases}
s_{lm} = \text{sign}(\sin \Phi_{lm}), & (20) \\
\alpha_{lm} = \text{sign}(\cos \Phi_{lm}), & (21) \\
w_{lm} = \left(\dfrac{1 - |\cos \Phi_{lm}|}{1 + |\cos \Phi_{lm}|} \right)^{1/2}, & (22)
\end{cases}
$$

with

$$
\Phi_{lm} = 4\pi(T_{lm} - t_R)/T_{\text{cyc}}. \tag{23}
$$

The normalized width of the cycle is the ratio between the minor and major axes of the *normalized* cycle $\delta\omega_{lm}/|\mathcal{J}_{lm}|$ as a function of R_Z/A_R. For the cycles shown in the upper panel of Fig. 4, the formulæ (20)–(22) correctly predict the circulation sense and inclination sign of the cycle, and values for the *normalized* width of 0.11 ($l = 0$), 0.04 ($l = 1$), 0.03 ($l = 2, m = 2$) and 0.53 ($l = 2, m = 0$). Now, the maximum of the activity indicator occurs less than 2 months before the maxima of the $l = 1$ and $l = 2, m = 2$ modes, but predates the maxima of the $l = 0$ and $l = 2, m = 0$ modes by about 5 and 20 months, respectively. This explains the different inclinations and widths of the resulting hysteresis cycles.

For the comparison of the foregoing with observational results like those of Jiménez-Reyes et al. (1998), one ought to obtain a composite measure of the frequency shift for all even-l modes, on the one hand, and all odd-l modes, on the other. To that end, we multiply the $\delta\omega_{lm}$ functions with the visibility factors v_{lm} of Christensen-Dalsgaard (1989) (as already done for the upper panel of Fig. 4), and add them together. The result is again a sinusoidal cycle in time with maximum at times T_{odd} and T_{even}, respectively. When plotted against the activity indicator, one obtains the cycles shown in Fig. 4, lower panel. The odd-l composite includes the $l = 3$ modes, which are not shown in the upper panel for the sake of clarity. Their contribution is anyway very small, as a result of the low values of their visibility factor.

The procedure followed here does not correspond exactly to the approach taken by Jiménez-Reyes et al. (1998), who obtained the frequency shifts from the location of the peak of the cross-correlation between power spectra obtained at different levels of activity. However, since the cross-correlation also weights the peaks according to their power, the two procedures should to first order give similar results. A more intricate analysis (i.e., one closer to that carried out by Jiménez-Reyes et al.) is not warranted, since it would unduly obscure the meaning and interpretation of the approach used in the present paper.

The circulation sense, inclination sign and normalized width of the composite cycles are given again by formulæ like (20)–(22), with Φ_{lm} now substituted by Φ, which is defined as

$$
\cos \Phi = \frac{C}{\sqrt{C^2 + S^2}}, \qquad \sin \Phi = \frac{S}{\sqrt{C^2 + S^2}}, \tag{24}
$$

with

$$
C = \sum_{l,m} v_{lm} |\mathcal{J}_{lm}| \cos \Phi_{lm},
$$

$$
S = \sum_{l,m} v_{lm} |\mathcal{J}_{lm}| \sin \Phi_{lm}. \tag{25}
$$

These formulæ correctly predict the circulation sense and inclination sign of the two composite cycles of Fig. 4, plus a normalized width of 0.09 for the even-l cycle and 0.04 for the odd-l cycle. Finally, in Fig. 5 we plot the frequency shifts of the odd modes, $\delta\omega_{\text{odd}}$, and of the even modes, $\delta\omega_{\text{even}}$, against each other. There results a cycle with normalized width 0.05, forward inclination and clockwise (i.e., positive) circulation, very similar to the results of Jiménez-Reyes et al. (1998); see their fig. 2. The cycle shown in Fig. 5 is not only scale-invariant, but also *independent of the choice of activity indicator*. This is very advantageous since the latter is rather arbitrary, bears no simple
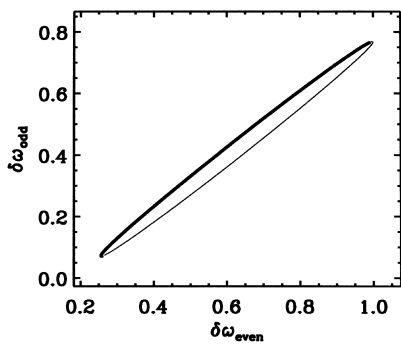
Figure 5. Frequency shift of the odd-*l* modes plotted against the frequency shift of the even-*l* modes. This plot is independent of the choice of activity indicator, and thus more fundamental than the cycles shown in Fig. 4.
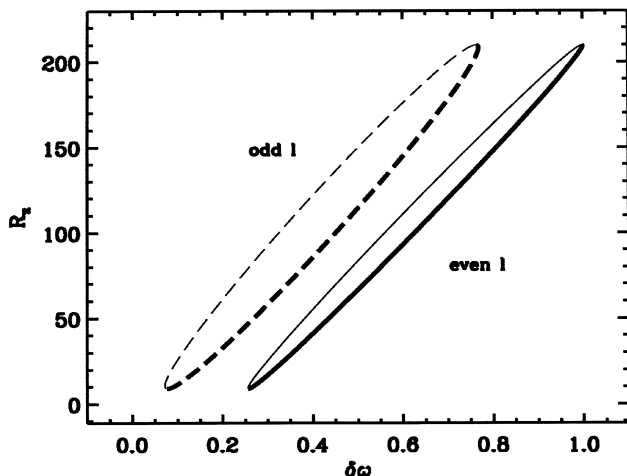
Figure 6. Composite odd- and even-degree hysteresis cycles for the same parameters as those underlying the cycles plotted in the lower panel of Fig. 4, but now artificially shifting the activity indicator by 5 months backward in time. The circulation sense of the hysteresis is now opposite to that of Fig. 4 (yet the width difference between the two cycles is conserved).

relationship to the surface distribution of magnetic flux, and introduces unnecessary observational noise into the problem. This is studied in the following subsection.

5.2 Dependence of the results on the activity indicator: invariant parameters

The choice of activity indicator may strongly influence the resulting hysteresis cycle. Equations (20)–(23), for instance, show explicitly how the inclination sign and circulation sense of a cycle depend on whether the proxy lags behind the $\delta\omega_{lm}$ of a particular mode, or runs ahead of it. An impression of the extent to which this can modify the cycles can be obtained through Fig. 6. In it we show the same composite cycles as in the lower panel of Fig. 4, but with the activity proxy artificially shifted backward in time by just 5 months. As can be seen, this small shift is sufficient to change the circulation sense of the cycles, although the width difference between them is preserved. Note, in particular, how the cycles obtained by Jiménez-Reyes et al. (1998) (their fig. 4) have the same circulation sense as those in the upper panel of our Fig. 4 (the width difference is also similar). If, instead of a time shift, we simply use a different proxy, like, e.g., the maximum of the

squared field distribution in the active latitudes at each instant or the integral of the square of the field over the whole hemisphere, then we also obtain a change of shape of the resulting cycles. The differences in this case would be due to the fact that the time evolution of the new activity indicator, though still cyclic, does not follow an exact sine curve; its extrema may also be somewhat shifted in time with respect to the indicator used for Fig. 4. In addition to all the foregoing considerations, the activity indicators obtained from the observations may suffer from saturation effects, etc. (as clearly visible in figs 3 and 4 of Jiménez-Reyes et al.). Also, the instrument and technique used on Kitt Peak to determine the magnetograms were qualitatively improved during the period studied by Jiménez-Reyes et al. In Appendix A we investigate the possible influence of these changes on the magnetic flux and its use as activity indicator.

To avoid the arbitrariness of the choice of activity indicator, it is of interest to introduce *invariant* parameters, i.e., parameters which are independent of (or only marginally dependent on) the amplitude or phase of the activity indicator. One such is the phase shift between two individual $\delta\omega_{lm}$ curves, $4\pi(T_{lm} - T_{l'm'})/T_{cyc}$. An approximate measure for this (valid to first order) can also be obtained directly from the cycle widths, $w_{lm}s_{lm} - w_{l'm'}s_{l'm'}$. Since currently only odd- and even-*l* modes can be distinguished with sufficient accuracy in the Tenerife data, the relative phase shift between the maxima of the odd and even composite cycles,

$$\Delta\Phi = 4\pi(T_{\text{odd}} - T_{\text{even}})/T_{\text{cyc}}, \tag{26}$$

and its associated width difference,

$$\Delta w = s_{\text{odd}}w_{\text{odd}} - s_{\text{even}}w_{\text{even}}, \tag{27}$$

are of immediate interest.

Since our analysis cannot predict the absolute value of the frequency change over the cycle, i.e., $\max(\delta\omega_{lm}) - \min(\delta\omega_{lm})$, it is of interest to consider plots which are scale-invariant, like the one in Fig. 5, as well as the associated invariant parameter

$$\Delta_{\max} = \frac{\max(\delta\omega_{\text{even}}) - \min(\delta\omega_{\text{even}})}{\max(\delta\omega_{\text{odd}}) - \min(\delta\omega_{\text{odd}})}, \tag{28}$$

which can be robustly determined from the observations, in particular those of Jiménez-Reyes et al. (1998). $\Delta_{\max}$ is the ratio of the frequency shift of the even modes to that of the odd modes.

5.3 Which power of *B* yields the observed hysteresis?

The cycles shown in Figs 4–6 all have an approximately elliptical shape, with small deviations due to the fact that the activity indicator does not follow an exact sinusoidal curve. Yet, a strong deformation (*bending*) of the ellipse would result if the sound-speed perturbation were proportional to the *B* function itself, and not to its square as assumed in the previous figures. The Lissajous curve corresponding to the composition of a sine with a sine-squared curve is still a closed curve with no internal crossings, which is somewhat reminiscent of an ellipse, although the major axis is now *bent* into a non-straight line. This can be seen in Fig. 7, which reproduces the calculation shown in Fig. 4, but now with the exponent $i_b = 1$ in equation (15).

In principle, the dependence on the exponent of *B* of the physical process which shifts the frequencies can be diagnosed from the curvature of the major axis of the hysteresis curve. Fig. 7 suggests that the canopy mechanism should give straight lines, while the interaction with flux tubes provides banana-shaped
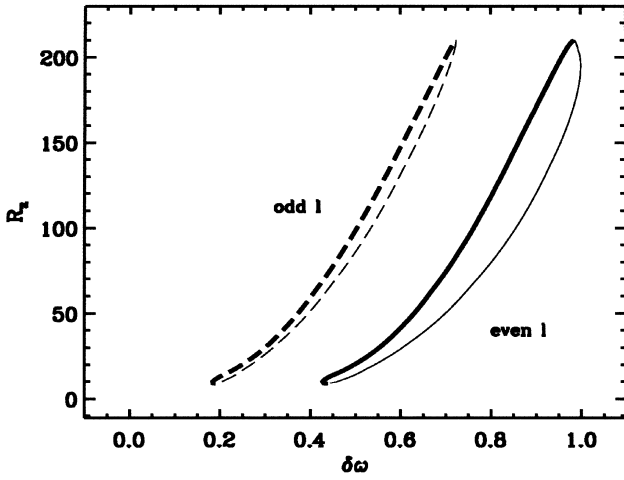
Figure 7. Hysteresis cycles assuming the sound-speed perturbation to be proportional to B instead of B^2 ($i_b = 1$ instead of 2 in equation 15). The activity indicator is once again R_Z and $n = 2$, $q = 0.7$ as in Fig. 4. The hysteresis cycles are now bent or *banana-shaped*.
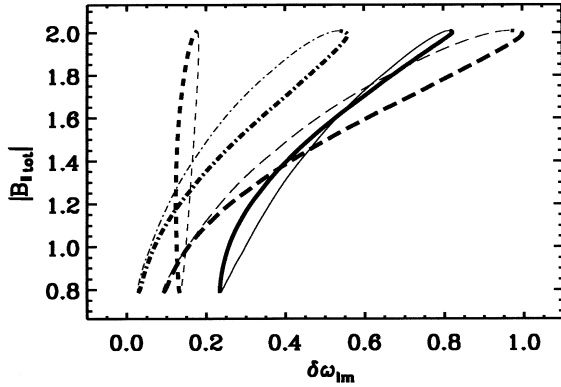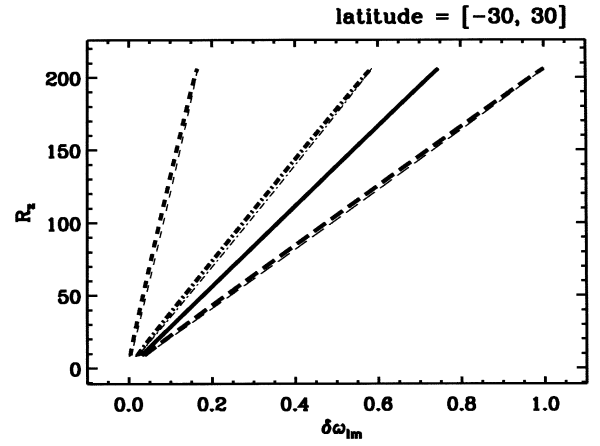

Figure 8. Hysteresis cycles obtained using as activity indicator the unsigned longitudinal magnetic field $|B_\parallel|$ given by equation (13). The *pistol* shape comes from the dependence on a different power of B of the frequency shifts (which are proportional to B^2 in these calculations) and activity indicator (proportional to B). Parameters and line styles as for Fig. 4.

curves. Unfortunately, it is not sufficient to compare these shapes with the observations in order to distinguish between the two theories, since the curvature of the hysteresis curves also depends significantly on the exact dependence of the chosen proxy on $B(\theta, t)$. For example, in Fig. 8 we plot exactly the same frequency shifts as in Fig. 4, but versus the longitudinal magnetic field (see equation 13) instead of versus R_Z. Note that the curves are now *pistol-shaped*.

5.4 Dependence on the latitude distribution of the magnetic flux

5.4.1 Dependence on high-latitude fields

The hysteresis cycles shown in Figs 4 and 6 are a direct consequence of the phase difference between the time evolution of the magnetic flux at different latitudes, together with the different dependence of the various (l, m) on the latitude. In particular, Fig. 4 leads us to suspect that fields at high latitudes also play an


Figure 9. Hysteresis cycles obtained by setting the magnetic field given by equation (10) to zero outside the activity belt ($|$latitude$| \geq 30°$), but otherwise keeping the same parameters of Fig. 4. The activity indicator used is R_Z. The cycles have now basically collapsed to straight lines. Line styles as for Fig. 3.

important role in determining the hysteresis. As a test of this statement, we consider an extreme case in which we artificially suppress the magnetic flux from all latitudes outside the activity belt by multiplying B of equation (10) with a window function that sets $B(\theta, t)$ equal to zero for latitudes λ with $|\lambda| > 30°$ (equation 11). According to the prediction of the foregoing sections, the even-mode and the odd-mode frequency shifts should then be in phase; the corresponding hysteresis cycles should therefore have the same circulation sense and width. Additionally, we expect the activity proxy R_Z to be roughly in phase with the frequency shifts (both now depend on the same fields), so that the width of both cycles should be close to zero.

This is indeed the case: Fig. 9 shows the hysteresis cycles obtained with the I_{lm} integrals of equation (8) calculated using (11). The cycles basically collapse to just a straight line, i.e., no hysteresis is left: the maxima in time of the activity indicator and frequency shifts are separated only by several days in most cases shown and less than one month in all of them. The ratio between minor and major axes (of the normalized cycles) is now below 0.01 for all modes except for $l = 2$, $m = 0$ for which it is 0.03. The width difference between odd and even composite cycles (which are not shown in the figure), Δw, is very small, 10^{-3}, as compared to 0.05 in Fig. 4. If we increase the phase shift of the proxy *by hand*, then the cycle width increases but Δw remains essentially zero. This test thus demonstrates that fields at latitudes outside the activity belts are essential for producing a *differential* hysteresis.

In spite of the marked change of shape of the cycles, the maximum frequency shift (relative to the fiducial value of a field-free Sun) does not change substantially when we suppress the fields outside the activity belt. This is because the maximum frequency shift coincides in time with the maximum of the field distribution close to the equator. At that time the high-latitude fields are small anyway, so the resulting frequency shift is not much affected by their suppression. On the other hand, the minimum frequency shift changes appreciably for those modes which are sensitive to the high-latitude fields, viz. the zonal modes $l = 0, m = 0$ and $l = 2, m = 0$. To a lesser extent this applies also to the sectoral mode $l = 1, m = 1$. This conclusion can also be checked by using a field distribution with $n = 0$ in equation (10)
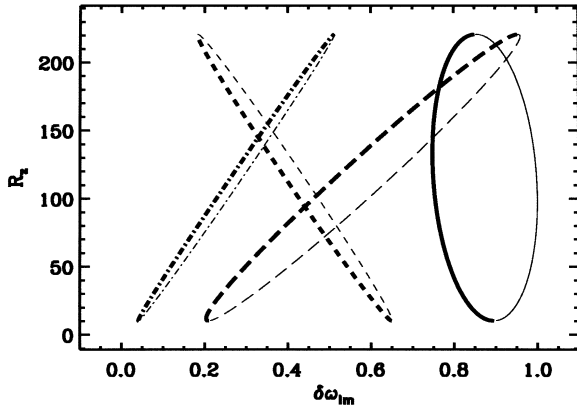
Figure 10. Hysteresis cycles for the individual modes corresponding to a magnetic field distribution with strong polar fields ($n = 0$ in equation 10). Note that, as a consequence, the frequency shift at cycle minimum for the modes with $m = 0$ is larger than at cycle maximum. These two curves exhibit backward inclination. Line styles as for Fig. 3.

(Fig. 10). It yields unduly strong polar fields, so that the frequency shift caused by them in fact overshoots the frequency shift due to the equatorial fields in the two zonal modes (2,0) and (0,0). For these modes the ellipses exhibit backward inclination. Of interest for the comparison with the observations is $\max(\delta\omega_{lm}) - \min(\delta\omega_{lm})$, since the fiducial frequency of the field-free Sun is a priori unknown.

In summary, the modes with $m = 0$ and their hysteresis cycles are very sensitive to the presence of high-latitude fields oscillating in phase opposition with the equatorial fields.

5.4.2 Behaviour of the invariant parameters

Given the uncertainties in the actual surface distribution of the magnetic structures that cause the shift in frequency of the low-l modes, it is convenient to study in a bit more detail the dependence of the invariant parameters characterizing the differential frequency shifts on the relative importance of the field in the low-, high- and mid-latitude regions. The two relevant parameters in this case are n and q in equation (10) via the factor $F_{n,q}(\theta) = |\cos^n[q(\pi/2 - \theta)]|$. For $n = 0$ or $q = 0$ we have Stenflo's original distribution (9), which yields very strong polar fields. For $n = 1$ and $n = 2$, the parameter q controls the gradual suppression of the polar fields as q grows upward from $q = 0$, or diminishes downward from $q = 2$. Fig. 11 illustrates the influence of q for the case $n = 2$. $q > 1$ corresponds to the suppression of the mid-latitude fields, whereas for $q < 1$ $F_{n,q}(\theta)$ steadily declines from 1, at the equator, to a value between 0 and 1 at the poles. Choosing $n = 2$, finally, causes the suppression of mid- or high-latitude fields to extend to a wider range of latitudes than if $n = 1$ had been chosen for the same q.

The invariant parameters react sensitively to the different patterns of surface field corresponding to the various values of q. This can be seen in Fig. 12 (upper panel), where we show the phase shift $\Delta\Phi$ between the maxima of odd- and even-degree hysteresis cycles (equation 26), together with the amplitude ratio $\Delta_{\max}$ defined in equation (28). The corresponding values of the width difference Δw (equation 27) are shown in the lower panel. $n = 0$ (or, equivalently, $q = 0$) yields large values of the time delay and associated width difference, much larger than in the observational results of Jiménez et al. (1998). At the opposite
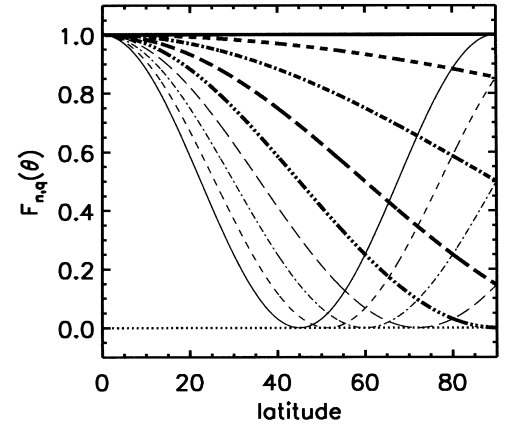
Figure 11. The form factor $F_{n,q}(\theta) = |\cos^n[q(\pi/2 - \theta)]|$ for $n = 2$ and different values of q. The line codes are as follows: the line is drawn thick if $q \leq 1$, it is thin otherwise. A solid line corresponds to either $q = 0$ or $q = 2$, short-dashed to either $q = 0.25$ or $q = 1.75$, dot-dashed to $q = 0.5$ or $q = 1.5$, and long-dashed to either $q = 0.75$ or $q = 1.25$, the line with dashes followed by three dots, finally, is the curve for $q = 1$.
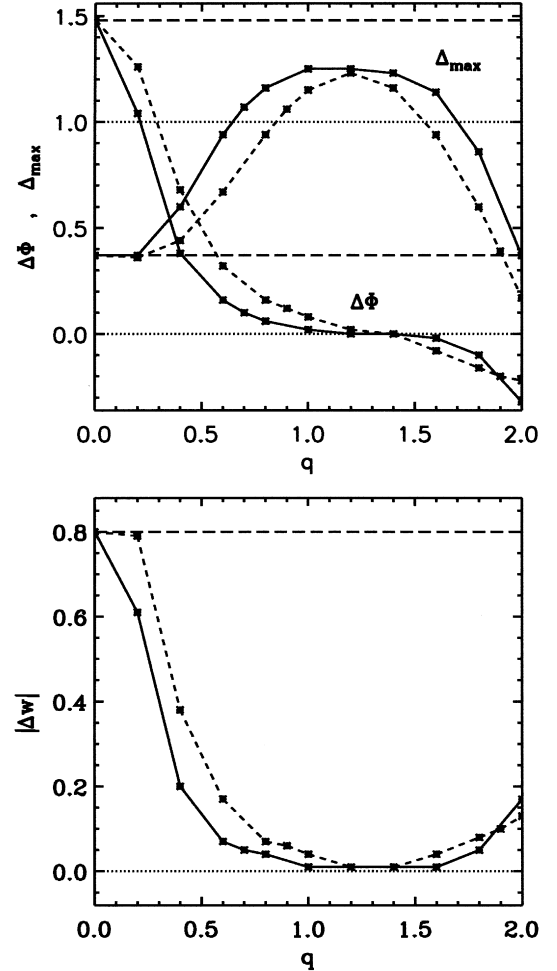
Figure 12. Top: invariant parameters $\Delta\Phi$ and $\Delta_{\max}$ characterizing the hysteresis cycles for different magnetic field distributions on the solar surface. Bottom: the corresponding width difference. Line styles are: $n = 2$: solid, $n = 1$: short-dashed, $n = 0$: long-dashed. (Note that for $n = 0$ the field distribution is unaffected by q.)

extreme, values of q between 1 and 1.5 imply the suppression of the high-latitude fields to an extent which brings the differential hysteresis between odd and even modes very close to zero (see, especially, the curve for $n = 2$).

The amplitude ratio Δ_{max} reaches a value of about 1.25 when the phase and width differences are zero. This is the same value that this parameters reaches when the high-latitude fields are artificially suppressed (Section 5.3). That it is greater than zero is a consequence of the greater effective power of the even-l modes in the active latitude belt compared to the odd-l modes (both for $l \leq 3$), when modulated with the visibility factors v_{lm}. Vice versa, as explained in Section 5.3, the presence of large polar fields raises the minimum frequency shift of the even modes while not modifying strongly the maximum frequency of any mode. Hence, for small q, the even-mode amplitude diminishes markedly, and a low value for Δ_{max} of about 0.35 ensues.

The right-hand end of the diagram (q close to 2) corresponds to high polar fields (as high as for $n = 0$) with simultaneous reduction of the field in the mid-latitudes (say, between 30° and 60°). The high polar fields make the zonal mode amplitude shrink to low values (hence the low Δ_{max}). On the other hand, the suppression of a large fraction of the mid-latitude fields, which otherwise contribute to the phase shift between sectoral and zonal modes, keeps the differential width at reduced values, well below the level of the $n = 0$ curve.

A comparison of the curves in Fig. 12 with the observed parameters, as estimated from the data of Jiménez-Reyes et al. (1998), (viz. $\Delta_{max} \approx 0.9$, $\Delta w \approx 0.05$ to 0.1) allows us to limit the free parameters to the following regions. For $n = 1$, q must lie in one of the two ranges (roughly 0.75 to 0.9 or 1.6 to 1.7), whereas for $n = 2$, the allowed q ranges are approximately 0.55 to 0.7 and around 1.8. Although there are four sets of parameters, they basically fall into two types of magnetic distributions, since the allowed field distributions for $n = 1$ are very similar to the respective distributions for $n = 2$. Therefore we need only distinguish between the cases $q < 1$ and $q > 1$. The main difference between these cases is that the high-latitude fields for $q < 1$ are more evenly distributed in latitude, while those for $q > 1$ are more strongly concentrated towards the poles. Both parameter regimes are equally allowed by the helioseismic observations. However, for $q > 1.5$ the polar fields become extremely strong and contradict the estimates obtained from magnetograms, which suggest that they are considerably weaker than active-region fields. As a result of the foregoing, $q \sim 0.7$ seems to be the optimum choice for $n = 2$ ($q \sim 0.8$ for $n = 1$).

6   DISCUSSION

Data for the frequency shifts of low-degree p-modes have now been collected for over a whole solar cycle. In the present paper we investigate the influence of the change in strength and surface distribution of solar magnetic fields on the frequency shifts $\delta\omega_{lm}$. In particular, we have studied the ability of diagrams in which $\delta\omega_{lm}$ is plotted versus some proxy of the solar magnetic field (such as sunspot number or average longitudinal flux) to distinguish between different magnetic field distributions. Of special interest are also plots of oscillation frequencies of different modes versus each other, which do not involve any measured proxy of the solar magnetic field. Such cycles are characterized by *invariant parameters* like the amplitude ratio Δ_{max} or the phase difference $\Delta\Phi$. The values of these parameters obtained from our

model can also be checked against the values obtained from the helioseismological data.

We have varied different parameters describing the magnetic field distribution on the solar surface, and have considered their influence on the p-mode frequency shifts. We find a set of parameters describing the magnetic distribution (or butterfly diagram) which produces synthetic p-mode frequency shifts that are approximately consistent with the observations. The magnetic distribution itself also appears reasonable. These suggest that intermediate-latitude fields (30°–70°) are just as important for the hysteresis as the polar fields. However, the ratio of the maximum frequency shifts (Δ_{max}) is much too large, unless sizable polar fields are present at activity minimum.

If the theoretical premises underlying our analysis are correct, then with improved observations of the type described by Jiménez-Reyes et al. (1998) (and improvements in the modelling; see below), it should be possible to identify at least some of the main characteristics of the butterfly diagram of solar magnetic fields. In particular, a differential analysis of the frequency shifts of different low-degree modes can provide information on the distribution of high-latitude fields.

Of course, polarimetric observations give much more direct and vastly more detailed information on, e.g., the fine-scale structure of the surface field. Nevertheless, helioseismic determinations of the solar field distribution has, in principle, some striking advantages. First, it is the magnetic field strength (and the magnetic filling factor, in a simple two-component model of the field) which is expected to affect the atmosphere and thus the oscillation frequencies. Hence the signal of the magnetic field does not suffer from cancellation of polarities, which plague magnetograms. Consequently, the oscillation method is independent of the spatial resolution of the observations. Secondly, the oscillation frequencies do not just sample the line-of-sight component of the field as full-disc magnetograms, such as those made daily at Kitt Peak do, nor do they suffer from foreshortening effects. They sample fields behind the solar limb as efficiently as those on the visible hemisphere. In addition, at least some modes (e.g., $m = 0$, i.e., zonal modes) are rather sensitive to the polar regions. This last point is particularly important, since magnetograms provide us with only relatively poor information on polar fields. This difference in sensitivity to the polar regions is illustrated in fig. 2 of Woodard & Libbrecht (1993).

Nevertheless, there are still a number of uncertainties in our analysis, foremost among which is the still open question of the type of magnetic structures responsible for the p-mode frequency shifts. For example, is it small photospheric flux tubes or chromospheric magnetic canopies, or even changes in the stratification of the field-free gas?

Our analysis has shown the possible pitfalls that may be present when frequency shifts are compared simply with a global activity parameter, such as sunspot number or average magnetic field strength, since the distribution of the magnetic field, which enters only very indirectly into such indices, can also affect the resulting frequency shifts. The quality of the correlation with a certain activity index (cf. Bachmann & Brown 1993) is not a sufficient measure of the importance for the p-mode shifts of the physical processes underlying that index. In contrast, the invariant parameters discussed in this paper (Sections 5.2 and 5.4.2) provide a much more reliable indicator.

How could we improve and extend the analysis further? One possibility which we have not considered is that, when constructing the frequency shifts of the odd and even l modes, the strengths

of the various l and m modes contributing to each could be different functions of the magnetic field strength and (to a smaller extent) distribution. As Pallé, Régulo & Roca Cortés (1990) and Elsworth et al. (1993) have shown, there is a strong trend towards reduced mode power at sunspot maximum (the modes change by, on average, 30–40 per cent in strength). Hence if, e.g., $l = 2, m = 0$ were to vary much less in strength than, say, $l = 2, m = 2$ over the solar cycle, then the hysteresis curves of the even-degree modes would be affected (in the sense that the hysteresis would be larger). Unfortunately, the data of Pallé et al. (1990) and Elsworth et al. (1993) are not of sufficient accuracy to allow us to test this possibility in detail.

Another improvement to the model would be to use synoptic maps constructed directly from the Kitt Peak magnetograms. However, prior to this the corrections to be made to the magnetograms in order to obtain the unsigned flux at all latitudes need to be worked out in detail.

The frequency shifts of intermediate-degree modes predicted by our model relative to those of the low-degree modes provide yet another test. Shibahashi (1997) has shown that for a magnetic field concentrated at the active latitudes the frequency shifts of low- and intermediate-degree modes are indeed consistent with each other. Note that the magnetic distribution which is successful in reproducing the observations also possesses a strong concentration of the field towards the active latitudes. Nevertheless, in a future step this test should be carried out. Even better would be to invert the frequency shifts and/or splittings of both low- and intermediate-degree modes in order to set tighter constraints on the time-dependent distribution of magnetic flux (or rather the magnetic energy).

Finally, we expect a systematic study of the influence of distinctly non-solar surface distributions of magnetic flux to provide a useful guide to the possibilities presented by future p-mode observations of stars to constrain their magnetic butterfly diagrams.

ACKNOWLEDGMENTS

REFERENCES

Bachmann K. T., Brown T. M., 1993, ApJ, 411, L45
Bachmann K. T., White O. R., 1994, Solar Phys., 150, 347
Bogdan T. J., Zweibel E. G., 1985, ApJ, 298, 867
Chapman G. A., Cookson A. M., Dobias J. J., 1997, ApJ, 482, 541
Christensen-Dalsgaard J., 1989, MNRAS, 239, 977
Christensen-Dalsgaard J., 1998, Lecture Notes on Stellar Oscillations. Aarhus Universitet, Denmark
Dziembowski W. A., Goode P. R., 1997, A&A, 317, 919
Dziembowski W. A., Goode P. R., Schou J., Tomczyk S., 1997, A&A, 323, 231
Elsworth Y., Howe R., Isaak G. R., McLeod C. P., New R., 1990, Nat, 345, 322
Elsworth Y., Howe R., Isaak G. R., McLeod C. P., Miller B. A., New R., Speake C. C., Wheeler S. J., 1993, MNRAS, 265, 888
Elsworth Y., Howe R., Isaak G. R., McLeod C. P., Miller B. A., New R., Speake C. C., Wheeler S. J., 1994, ApJ, 434, 801
Evans D. J., Roberts B., 1990, ApJ, 356, 704
Evans D. J., Roberts B., 1991, ApJ, 371, 387
Evans D. J., Roberts B., 1992, Nat, 355, 230
Fröhlich C., Lean J., 1998, in Deubner F. L., ed., Proc. IAU Symp. 185, New Eyes to See Inside the Sun and Stars. Kluwer, Dordrecht, p. 89
Gelly B. et al., 1997, A&A, 323, 235
Giovanelli R. G., 1982, Solar Phys., 77, 27
Goldreich P., Murray N., Willette G., Kumar P., 1991, ApJ, 370, 752
Gough D. O., 1988, in Rolfe E. J., ed., Seismology of the Sun and Sun-like Stars. ESA SP-286, p. 679
Gough D. O., Taylor P. P., 1984, Mem. Soc. Astron. Ital., 55, 215
Gough D. O., Thompson M. J., 1988a, in Christensen-Dalsgaard J., Frandsen S., eds, Proc. IAU Symp. 123, Advances in Helio- and Asteroseismology. Reidel, Dordrecht, p. 155
Gough D. O., Thompson M. J., 1988b, in Christensen-Dalsgaard J., Frandsen S., eds, Proc. IAU Symp. 123, Advances in Helio- and Asteroseismology. Reidel, Dordrecht, p. 175
Gough D. O., Thompson M. J., 1990, MNRAS, 242, 25
Grossmann-Doerth U., Pahlke K.-D., Schüssler M., 1987, A&A, 176, 139
Harvey K. L., 1991, in Donnelly R. F., ed., Proc. of the Workshop on the Solar Electromagnetic Radiation Study from Solar Cycle 22, NOAA, US Dept. of Commerce, p. 113
Howard R., LaBonte B. J., 1981, Solar Phys., 74, 131
Jain R., Roberts B., 1993, ApJ, 414, 898
Jiménez-Reyes S. J., Régulo C., Pallé P. L., Roca Cortés T., 1998, A&A, 329, 1119
Jones H. P., Duvall T. L. Jr., Harvey J. W., Mahaffey C. T., Schwitters J. D., Simmons J. E., 1992, Solar Phys., 139, 211
Kuhn J. R., 1988, ApJ, 331, L131
Kyle H. L., Hoyt D. V., Hickey J. R., 1994, Solar Phys., 152, 9
Libbrecht K. G., Woodard M. F., 1990, Nat, 345, 779
Lydon T. J., Guenther D. B., Sofia S., 1996, ApJ, 456, L127
Moreno-Insertis F., Schüssler M., Ferriz-Mas A., 1992, A&A, 264, 686
Pallé P. L., 1994, in Ulrich R. K., Rhodes E. J. Jr., Däppen W., eds, ASP Conf. Ser. Vol. 76, GONG'94: Helio- and Astero-seismology from the Earth and Space. Astron. Soc. Pac., San Francisco, p. 239
Pallé P. L., Régulo C., Roca Cortés T., 1990, in Osaki Y., Shibahashi H., eds, Progress of Seismology of the Sun and Stars. Springer-Verlag, Berlin, p. 129
Paternò L., 1990, in Osaki Y., Shibahashi H., eds, Progress of Seismology of the Sun and Stars, Lecture Notes in Physics, Vol. 367. Springer-Verlag, Berlin, p. 41
Rees D. E., Semel M. D., 1979, A&A, 74, 1
Rhodes E. J. Jr, Cacciani A., Korzennik S. G., Ulrich R. K., 1993, ApJ, 406, 714
Rüedi I., Solanki S. K., Livingston W., Stenflo J. O., 1992, A&A, 263, 323
Schüssler M., Caligari P., Ferriz-Mas A., Moreno-Insertis F., 1994, A&A, 281, L69
Semel M., 1971, in Howard R. F., ed., Proc. IAU Symp. 43, Solar Magnetic Fields. Reidel, Dordrecht, p. 37
Sheeley N. R. Jr, Wang Y.-M., Harvey J. W., 1989, Solar Phys., 119, 323
Shibahashi H., Takata M., 1997, in Provost J., Schmider F.-X., eds, Proc. IAU Symp. 181, Sounding Solar and Stellar Interiors. Kluwer, Dordrecht, p. 167
Solanki S. K., Zuffrey D., Lin H., Rüedi I., Kuhn J., 1996, A&A, 310, L33
Stenflo J. O., 1970, Solar Phys., 13, 42
Stenflo J. O., 1972, Solar Phys., 23, 307
Stenflo J. O., 1994, in Rutten R. J., Schrijver C. J., eds, Solar Surface Magnetism. Kluwer, Dordrecht, p. 365
Svalgaard L., Duvall T. L. Jr., Scherrer P. H., 1987, Solar Phys., 58, 225
Tassoul M., 1980, ApJS, 43, 469
Vandakurov Yu. V., 1967, SvA, 11, 630
Vorontsov S. V., 1988, in Christensen-Dalsgaard J., Frandsen S., eds, Proc. IAU Symp. 123, Advances in Helio- and Asteroseismology. Reidel, Dordrecht, p. 151

Willson R. C., Hudson H. S., 1991, Nat, 351, 42
Woodard M. F., Libbrecht K. G., 1993, ApJ, 402, L77
Woodard M. F., Noyes R. W., 1985, Nat, 318, 449
Woodard M. F., Kuhn J. R., Murray N., Libbrecht K. G., 1991, ApJ, 373, L81
Wright A. N., Thompson M. J., 1992, A&A, 264, 701
Zhang L. D., Zirin H., Marquette W. H., 1997, Solar Phys., 175, 59
Zweibel E. G., Däppen W., 1989, ApJ, 343, 994

APPENDIX A: COULD THE HYSTERESIS PARTLY HAVE AN INSTRUMENTAL ORIGIN?

In cycle 22 (over which the helioseismology data were mainly gathered) there is a clear hysteresis between the line-of-sight magnetic flux, φ_{LOS}, and R_Z, but no such hysteresis is visible in cycle 21 (cf. Harvey 1991). Note that hysteresis between various solar activity indicators is common (Bachmann & White 1994), so that the presence or absence of such a hysteresis is not in itself remarkable. The difference between the two cycles is, however, unexpected.

Here we test whether this difference between cycles 21 and 22 is solar, or whether the instruments or techniques used to observe these quantities evolved in the course of these two cycles. Of particular concern are changes to the magnetic field measurement technique in the course of cycle 22, since this could produce an artificial hysteresis between R_Z and φ_{LOS}, and thus also between $\delta \nu$ and φ_{LOS}.

There has indeed been a change in instrumentation in the course of cycle 22. The old 512-channel magnetograph at the solar tower telescope on Kitt Peak was replaced by the spectromagnetograph (Jones et al. 1992). The new instrument has various advantages over the older one. For example, it does not saturate in sunspots. Also, the use of the centre-of-gravity technique (Semel 1971; Rees & Semel 1979) allows more reliable flux values to be determined (Grossmann-Doerth, Pahlke & Schüssler 1987). All in all, we expect the new system to detect a larger fraction of the solar φ_{LOS}, so that newer measurements of φ_{LOS} are expected to show larger values than older measurements. This expectation is supported by the initial comparisons carried out by Jones et al. (1992). In principle, this effect could create an artificial hysteresis. Although the determination of the exact factor by which the detection efficiency increases would require a detailed analysis, we can nevertheless test this hypothesis by *assuming* that the new spectromagnetograph detects 20 per cent more flux than its predecessor (this estimate is probably too large, but we have
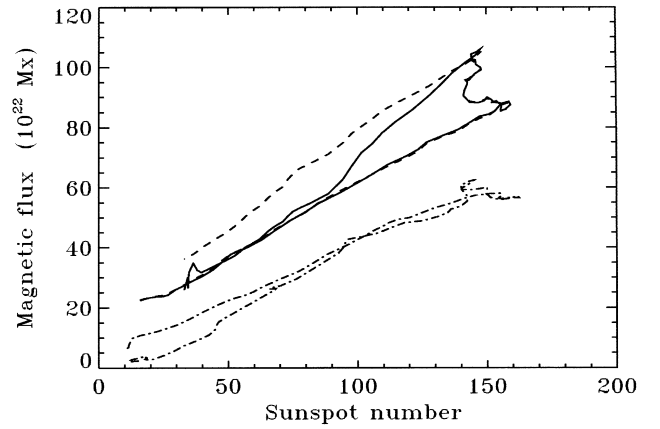
Figure A1. Longitudinal magnetic flux obtained from Kitt Peak magnetograms versus sunspot number, R_Z. Plotted are the results for solar cycles 21 (dot-dashed curve) and 22 (dashed curve). The curve for solar cycle 21 has been vertically offset by 2×10^{23} Mx for clarity. The solid curve represents solar cycle 22 under the assumption that the new Kitt Peak spectromagnetograph observed 20 per cent more flux than the old linear-array magnetograph. All curves have been smoothed by a running mean.

deliberately chosen to err in this direction in order to demonstrate the effect clearly). We then decreased the flux by 20 per cent from 1992 April 21 onwards. In Fig. A1 we plot both the original (dashed) and the artificially changed (solid) φ_{LOS} versus R_Z relationship. The hysteresis of the changed relationship is significantly reduced at small R_Z, but is practically unaffected near the peak of the cycle. This is because the changeover to the new system occurred well after the peak of cycle 22, which was in 1989–90 in sunspot numbers and in 1991 in magnetic fields. (Note that the change in the high-R_Z part of the decreasing leg of the cycle 22 is mainly due to the 1-year running mean used to smooth the data.)

In summary, although it is conceivable that the φ_{LOS} versus R_Z hysteresis is less pronounced than is apparent directly from the data, it cannot be entirely due to instrumental effects. Consequently, any statistically significant hysteresis between $\delta \nu$ and φ_{LOS} is in all probability also real. A difference between the two cycles also remains.

This paper has been typeset from a TeX/LATeX file prepared by the author.